

# Nanostructured nickel electrodes using the *Tobacco mosaic virus* for microbattery applications

Konstantinos Gerasopoulos<sup>1</sup>, Matthew McCarthy<sup>1</sup>, Elizabeth Royston<sup>2</sup>, James N Culver<sup>2</sup> and Reza Ghodssi<sup>1</sup>

<sup>1</sup> MEMS Sensors and Actuators Laboratory (MSAL), Department of Electrical and Computer Engineering, Institute for Systems Research, University of Maryland, College Park, MD 20742, USA

<sup>2</sup> Center for Biosystems Research, University of Maryland Biotechnology Institute, University of Maryland, College Park, MD 20742, USA

E-mail: [ghodssi@umd.edu](mailto:ghodssi@umd.edu)

Received 4 April 2008, in final form 12 June 2008

Published 29 September 2008

Online at [stacks.iop.org/JMM/18/104003](http://stacks.iop.org/JMM/18/104003)

## Abstract

The development of nanostructured nickel–zinc microbatteries utilizing the *Tobacco mosaic virus* (TMV) is presented in this paper. The TMV is a high aspect ratio cylindrical plant virus which has been used to increase the active electrode area in MEMS-fabricated batteries. Genetically modifying the virus to display multiple metal binding sites allows for electroless nickel deposition and self-assembly of these nanostructures onto gold surfaces. This work focuses on integrating the TMV deposition and coating process into standard MEMS fabrication techniques as well as characterizing nickel–zinc microbatteries based on this technology. Using a microfluidic packaging scheme, devices with and without TMV structures have been characterized. The TMV modified devices demonstrated charge–discharge operation up to 30 cycles reaching a capacity of  $4.45 \mu\text{Ah cm}^{-2}$  and exhibited a six-fold increase in capacity during the initial cycle compared to planar electrode geometries. The effect of the electrode gap has been investigated, and a two-fold increase in capacity is observed for an approximately equivalent decrease in electrode spacing.

(Some figures in this article are in colour only in the electronic version)

## 1. Introduction

A major challenge towards the realization of autonomous integrated microsystems is power generation and energy storage. Wireless sensor networks need compact on-chip power for various electronic components and energy harvesting devices require efficient storage mechanisms. As these systems are scaled down, the available surface area limits the performance of microbatteries. Accordingly, active research is being conducted to enhance power generation and energy storage devices through high surface area electrode structures.

Initial work in the field of MEMS-fabricated batteries focused on the development of planar (thin-film) electrode designs, using traditional micromachining processes. Lee and Lin demonstrated a disposable microbattery in a

parallel-plate configuration with a zinc anode and a gold cathode [1]. The microbattery was fabricated with surface micromachining techniques and adhesive bonding. Humble *et al* fabricated and characterized nickel–zinc microbatteries with electroplated active materials in a side-by-side configuration [2]. While these cells use aqueous electrolytes, researchers have successfully developed lithium-based thin-film batteries using a lithium phosphorus oxynitride solid electrolyte [3, 4].

In addition to thin-film approaches, microfabrication techniques have also been used to create three-dimensional microbatteries. In these architectures, the electrodes have high aspect ratio out-of-plane microstructures, resulting in an increased surface area while maintaining device footprint [5]. Wang *et al* demonstrated the use of carbon electrodes made of pyrolyzed SU-8 posts for lithium batteries [6], while

Chamran *et al* presented high aspect ratio posts for nickel–zinc and lithium-ion batteries based on molding in silicon and electroplating or colloidal processing [7].

To further increase the reactive surface area, the integration of nanomaterials and biological nanostructures has also been investigated. Zhang *et al* synthesized cathodes for lithium-ion batteries based on vanadium oxide ( $V_2O_5$ ) sol-gel coating of high aspect ratio carbon nanotubes [8], while flexible light weight batteries using nanoporous cellulose paper and embedded carbon nanotubes have also been demonstrated [9]. In the field of nickel–zinc batteries, the use of zinc oxide (ZnO) nanorods has been shown to increase the reactive surface area compared to conventional zinc oxide and improve the cycling performance [10]. The use of biological nanomaterials is an attractive approach for the fabrication of battery electrodes, as they exist in nature as high aspect ratio nanostructures, do not require bulky equipment for their synthesis and can be modified to bind to a variety of active battery materials. Hybrid gold–cobalt oxide nanowires based on engineered modifications of the M-13 bacteria virus have been synthesized and used as positive electrodes in a macroscopically assembled lithium ion battery [11]. Previous work by Royston *et al* reports the use of genetically modified *Tobacco mosaic virus* (TMV) as a template for electroless deposition of cobalt and nickel [12]. An order of magnitude increase in the surface area was estimated for the nanostructured nickel materials, and their potential as battery electrodes has been demonstrated through electrochemical experiments. The focus of this work is the integration of the TMV self-assembly and electroless nickel plating process into standard micromachining techniques for the development of MEMS-fabricated batteries.

## 2. Materials and chemistry

### 2.1. Tobacco mosaic virus

The TMV is a high aspect ratio cylindrical plant virus measuring 300 nm in length with an outer diameter of 18 nm and an inner diameter of 4 nm. A TEM image of wild-type viruses is shown in figure 1. Each TMV structure consists of approximately 2130 coat protein subunits wrapped around a positive-sense single-stranded ribonucleic acid ((+)-ssRNA) in a helical structure. The TMV is a robust biological structure, showing stability in temperatures up to 60 °C and pH values from 2 to 10 [12]. Additionally, it is renewable in large quantities and has well-defined assembly features that allow mineralization through repeatedly exposed amino acids around its surface [13]. Previous research has shown that genetically modifying the virus to introduce cysteine residues (amino acid with thiol groups) in its coat proteins significantly enhances metal deposition, which is attributed to covalent-like bonds formed between the thiol groups of the cysteines and various metal surfaces [14].

In this work we use the TMV1cys, an engineered mutant of the wild-type virus containing a cysteine residue in each of the coat proteins. This modification is achieved through a PCR-based site-directed mutagenesis process and has been

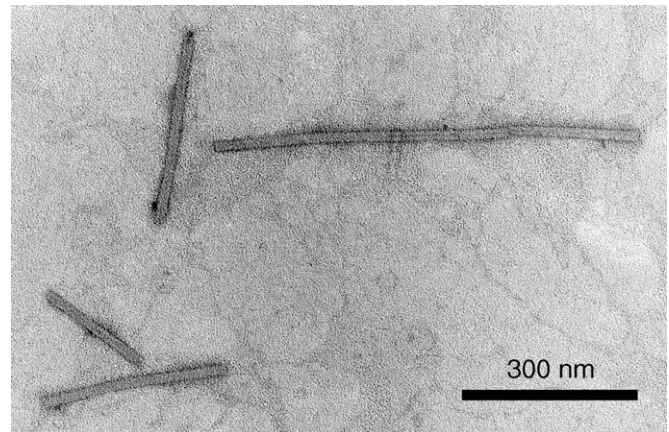


**Figure 1.** The TEM image of wild-type viruses with a magnification of 125 000.

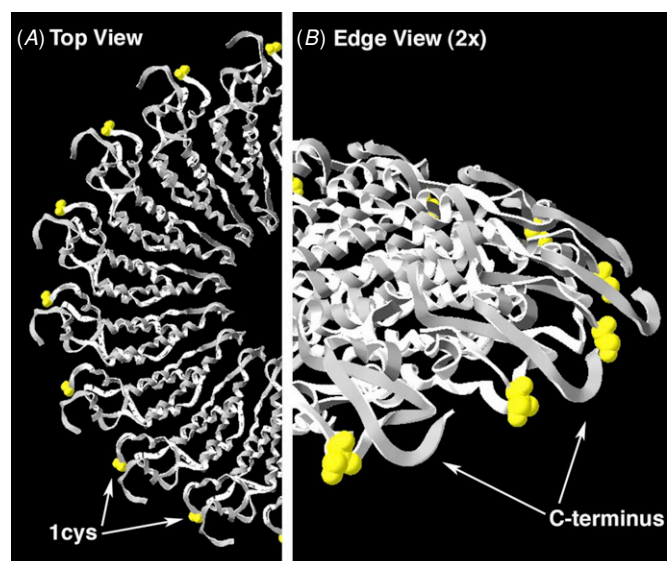


**Figure 2.** Structural location of the TMV1cys mutation. (a) Top view showing half of a coat protein layer within the TMV rod and (b) 2× magnification of an edge view for the same coat protein layer (location of the 1cys mutations are highlighted in yellow).

described in detail previously [15, 16]. A complementary DNA clone is produced from the wild-type viral RNA, and the specific cysteine codon is introduced in the third position of the coat protein open reading frame. Following this process, RNA transcripts are used to infect the host plant which acts as the factory for mass production of the virus, and finally the TMV1cys is harvested 20 days after inoculation [17]. A structural diagram of the alpha carbon traces for individual coat protein subunits is shown in figure 2. Figure 2(a) shows a top view of one virion with the cysteine residues around the surface. The exposed cysteines of the 3' end are demonstrated in the edge view given in figure 2(b).

### 2.2. Chemistry

The microbattery developed in this study uses a nickel–zinc chemistry with a potassium hydroxide (KOH) aqueous electrolyte. This is a secondary alkaline battery that can be constructed using standard MEMS fabrication processes. Its

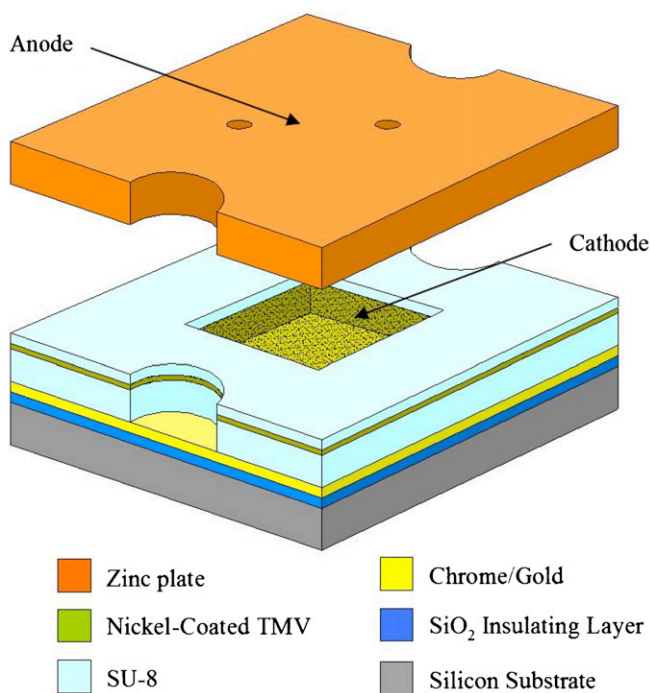


Figure 3. Schematic of the microbattery layers.

rechargeable nature allows it to be used in applications where many charge–discharge cycles are necessary.

Royston *et al* performed XPS elemental analysis of the nickel-coated TMV surface to investigate the composition of the nanostructured electrode [12]. Metallic nickel, nickel oxide (NiO) and nickel hydroxide (Ni(OH)<sub>2</sub>) were detected, suggesting that the following two reactions occur during battery operation:



The right direction of the arrow corresponds to the discharge portion of the cycle while the left direction represents the charge reaction. During charging, nickel hydroxide and metallic nickel are converted into nickel oxyhydroxide and nickel oxide, respectively. When the direction of the current is reversed and the battery is discharged, the zinc electrode is oxidized and the electrons are transferred from the external circuit to reduce the cathode active materials back to their previous state. The expected theoretical voltages for these two chemistries are 1.73 V and 1.5 V respectively, based on the standard electrode potentials of the active components [23].

### 3. Design and fabrication

#### 3.1. Device design

The microbattery device is comprised of two electrodes separated by an electrolyte cavity defined in SU-8. A three-dimensional view of the battery showing the different layers is illustrated in figure 3. The bottom electrode (cathode) consists of nickel-coated TMV nanostructures assembled on a gold

current collector and the top electrode (anode) is a zinc plate machined with macroscale techniques. The two layers are bonded through an intermediate thin SU-8 layer. Electrolyte is introduced via through-holes machined in the zinc (500  $\mu\text{m}$  in diameter). The electrochemical cell active areas are 0.36 cm<sup>2</sup>, 0.64 cm<sup>2</sup> and 1 cm<sup>2</sup> as defined by lithography and the overall footprint of the device is 2 cm  $\times$  2 cm to ensure a strong bond with the anode and facilitate testing of the various geometries. The separation between the electrodes is determined by the two SU-8 layers. The structural SU-8 layer was fabricated with thicknesses of 55  $\mu\text{m}$  and 100  $\mu\text{m}$  while the bonding layer was found to add to this spacing by approximately 10  $\mu\text{m}$ .

#### 3.2. TMV self-assembly and coating process

The TMV self-assembly and nickel metallization are solution-based reactions that take place at room temperature [12]. The process is completed in three steps, which include binding of the virus onto a gold surface through the surface-exposed thiols of the cysteines (step 1), activation of the TMV surface with palladium to catalyze the electroless plating reaction (step 2) and finally coating of the virus with nickel (step 3) [18, 19]. The electroless formation of palladium clusters and nickel active material uses ionic metal baths mixed with a reducing agent. A schematic of the process is shown in figure 4.

The gold surface is cleaned in a 1:1 mixture of acetone and ethanol in an ultrasonic bath for 15 min and then rinsed thoroughly with deionized water. After drying with nitrogen, the chip is immersed in a solution containing TMV1cys at a concentration of 0.3 mg mL<sup>-1</sup> in a 0.1 M sodium phosphate buffer at pH 7 and allowed to incubate overnight to maximize attachment of the nanostructures onto the substrate. During this stage, the viruses self-assemble onto gold through the exposed cysteines at the 3' end. It is hypothesized that the favorable attachment of the TMV is perpendicular to the substrate, because the cysteines of the outer surface are recessed within the pits and grooves of the virus structure and therefore not directly exposed to gold (figure 2). In practice, mechanisms such as head to tail alignment of virions, existence of broken TMV rods and random distribution within the solution result in divergence from an absolute vertical alignment [12].

Following the TMV assembly on the substrate, the surface-exposed cysteine residues are activated with a palladium catalyst through reduction of Pd<sup>2+</sup> to Pd<sup>0</sup> in the presence of a hypophosphite-reducing agent. More specifically, a 10 mM sodium tetrachloropalladate (Na<sub>2</sub>PdCl<sub>4</sub>) solution is mixed with a 0.1 M phosphate buffer in a 1:15 ratio and the reaction on the virus surface proceeds during a second overnight step in the dark. Palladium is used as a catalyst for the nickel plating process [18, 19].

The final step of the coating process uses a standard electroless nickel plating solution at pH 7 containing 0.1 M nickel chloride (NiCl<sub>2</sub>), 0.15 M sodium tetraborate (Na<sub>2</sub>B<sub>4</sub>O<sub>7</sub>) and 0.25 M glycine in the presence of 0.5 M dimethylamine borane ((CH<sub>3</sub>)<sub>2</sub>NHBH<sub>3</sub>) as the reductant [18, 19]. The plating bath is mixed with DI water in a 1:1 ratio and the gold

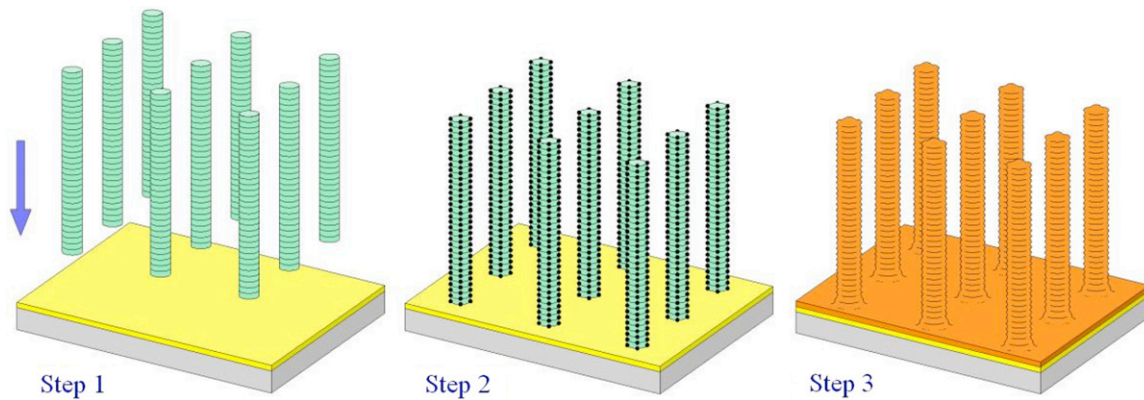


**Figure 4.** Schematic representation of the TMV assembly and nickel coating process: the TMV binds on the gold surface (step 1), it is activated with a palladium catalyst (step 2) and it is finally coated with nickel (step 3).

**Table 1.** Process parameters For a structural SU-8 layer.

	55 $\mu\text{m}$ thickness	100 $\mu\text{m}$ thickness
Spread cycle	600 rpm	600 rpm
	100 rpm s <sup>-1</sup>	100 rpm s <sup>-1</sup>
	10 s	10 s
Spin cycle	2500 rpm	1100 rpm
	270 rpm s <sup>-1</sup>	200 rpm s <sup>-1</sup>
	30 s	27 s
Soft bake	75 °C at	75 °C at
	5 °C min <sup>-1</sup>	5 °C min <sup>-1</sup>
	total of 40 min	total of 2 h and 15 min
Exposure dose	360 mJ cm <sup>-2</sup>	800 mJ cm <sup>-2</sup>
Post-exposure bake	75 °C	75 °C at
	5 °C min <sup>-1</sup>	5 °C min <sup>-1</sup>
	total of 35 min	total of 1 h and 15 min
Development	5 min	8 min

surface is immersed in the mixture for 2–3 min. At this point, nickel metal is directly reduced onto the palladium-catalyzed sites. Due to the autocatalytic nature of the nickel reaction, this electroless plating process results in a continuous nickel coating around the virus surface on the order of 20–40 nm [12].

### 3.3. Microbattery fabrication

The process begins with the deposition of a 0.5  $\mu\text{m}$  LPCVD silicon dioxide ( $\text{SiO}_2$ ) film on a silicon wafer. This dielectric layer is used to isolate the substrate from the cathode. Chrome and gold layers are then e-beam evaporated on the dielectric to thicknesses of 20 nm and 250 nm respectively. Chrome is used as an adhesion layer, while gold serves as the cathode current collector and the base for the TMV assembly.

The electrolyte cavity is fabricated using SU-8 50 (Microchem Corp.) in a single photolithography step. The polymer is spun to thicknesses of 55  $\mu\text{m}$  and 100  $\mu\text{m}$ . Due to the large area of the SU-8 structures, poor adhesion and crack formation were observed. This was addressed by decreasing the baking temperature as discussed in [20] from 95 °C to 75 °C and increasing the baking and ramping times, as well as the exposure dose. The process parameters for these two recipes are given in table 1. After SU-8 lithography, the wafers are diced to individual cathode layers and fabrication continues at

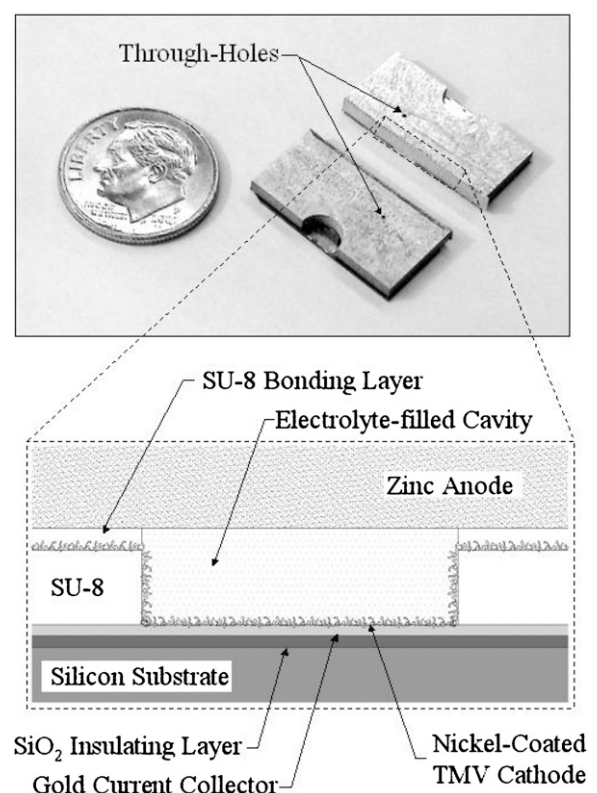


**Figure 5.** Image of a device diced in half and its cross sectional schematic.

the die level with the self-assembly and nickel coating of the TMV on the defined gold area as described in section 3.2.

The microfabricated bottom electrode is then bonded with the machined zinc anode using a stamp-and-stick process with an intermediate SU-8 layer. A thin SU-8 5 layer is spun at a final speed of 1600 rpm on a dummy silicon wafer. Directly after spinning, the die is pressed against the wafer transferring a thin viscous SU-8 layer to the structural SU-8 film. The zinc anode is then manually aligned with the cathode and the assembled device is baked on a hotplate at 100 °C with a ramp of 5 °C min<sup>-1</sup> for 5–10 min to strengthen the bond. In addition to bonding, this thin SU-8 layer electrically isolates the two electrodes, since TMV was found to adhere

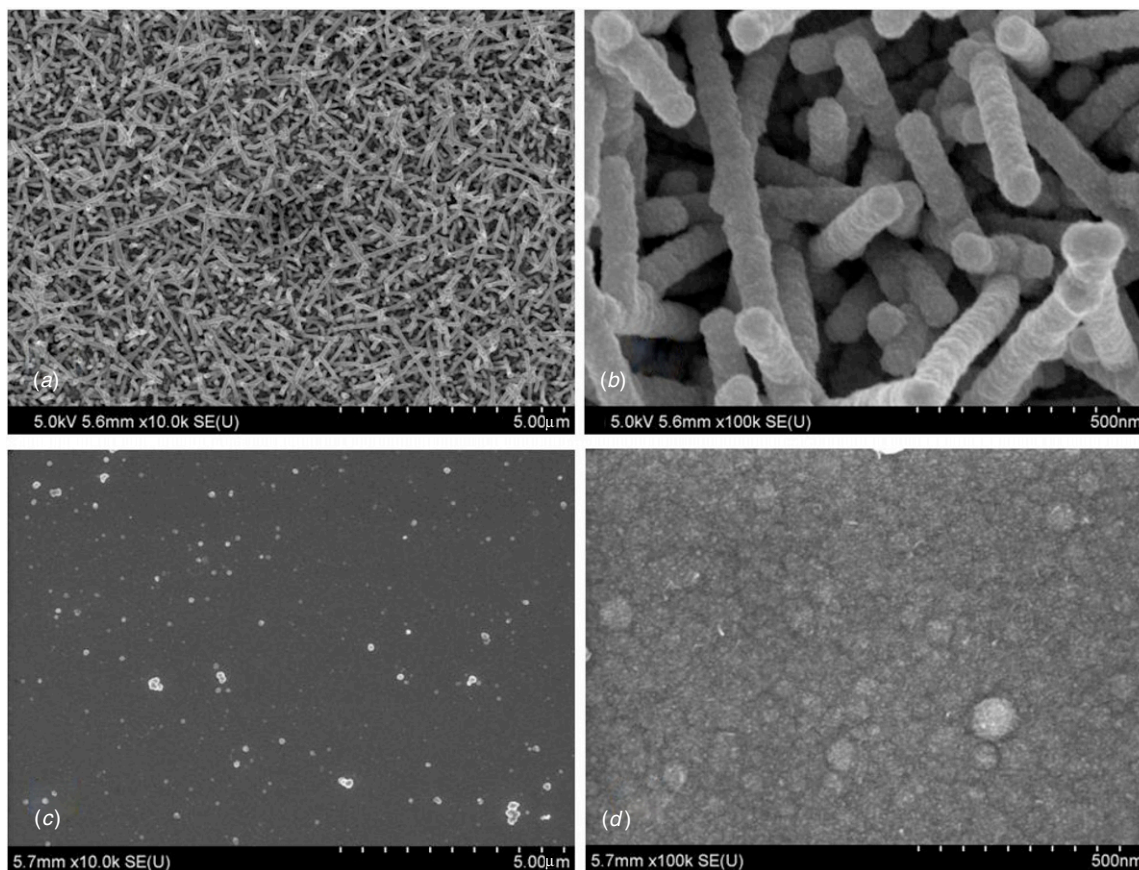


**Figure 6.** SEM images at two magnifications of nickel electrodes with ((a), (b)) and without ((c), (d)) TMV coatings.

to SU-8 as well. The thickness of this bonding layer was measured in various test devices and was found to be  $10\ \mu\text{m}$  in average. Figure 5 shows an image of a device diced in half and its cross sectional schematic. Microbatteries without viral nanostructures were fabricated using an identical process, excluding the TMV assembly. Figure 6 shows SEM images of nickel electrodes with and without TMV coatings, where a significant increase in the reactive area is evident. As was anticipated, the mechanisms described in section 3.2 prevented full vertical alignment of the viruses.

#### 4. Testing apparatus

A novel packaging scheme that allows testing of various device geometries was developed and is shown in figure 7. The package consists of two plastic manifolds made of LEXAN and held together with bolts. The bottom component serves as a base for the microbatteries while the top piece contains multiple fluidic ports for electrolyte circulation. The microbattery is placed on a rubber film at the base of the package for mechanical stability and electrical isolation. Two rubber o-rings are aligned with the holes machined in the zinc anode to ensure sealing and four additional identical o-rings are placed in each corner for mechanical support. The top piece is then aligned and held in place with bolts. The electrolyte is introduced manually using a syringe and electrical connections with the battery terminals are made with alligator clips.

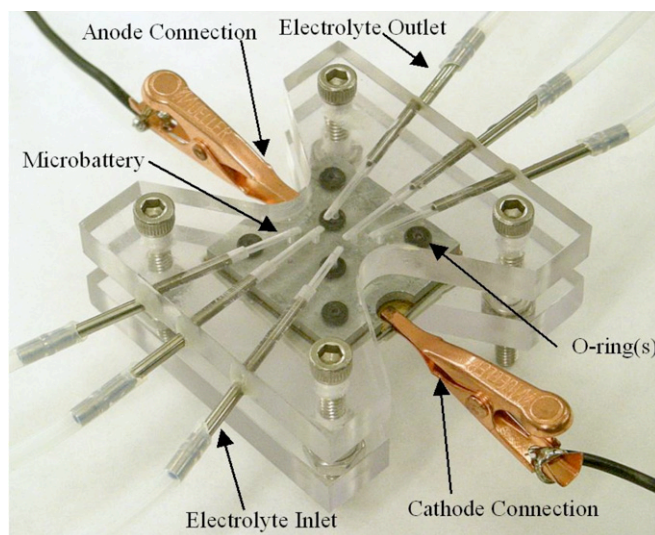


**Figure 7.** Image of a packaged microbattery showing the fluidic and electrical connections.

The devices are tested using a potentiostat (Solartron, model 1287A, Hampshire, UK) and commercial software for electrochemical analysis (Corrware, Solartron, Hampshire, UK). A potentiostat charges and discharges the battery at a constant current density within pre-determined voltage or time limits. During the charge cycle, current is provided to the device through the electrical connections for a pre-set time

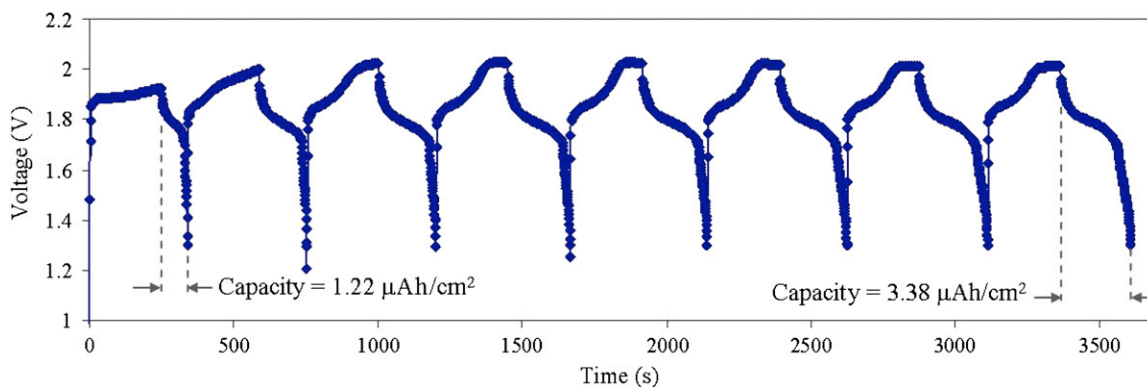


**Figure 8.** The charge–discharge curve of a TMV microbattery showing capacity for the first and eighth cycles of operation.

**Table 2.** Potentiostat parameters.

Programmed operation	15 cycles
Upper voltage limit	2.5 V
Lower voltage limit	1.3 V
Charge current density	100 $\mu\text{A cm}^{-2}$
Discharge current density	50 $\mu\text{A cm}^{-2}$
Charge time limit	250 s
Discharge time limit	500 s

or until the upper voltage limit is reached. When either of these two conditions is met, the discharge begins. During this process, current is drawn from the battery terminals until a lower voltage limit is reached or until the discharge exceeds the time set by the operator. The capacity is calculated by the product of the discharge time and the current and it represents the total charge generated during the reaction [23].

The parameters used for the electrochemical characterization of the microfabricated devices are summarized in table 2. The upper and lower voltage limits as well as the times for the charge and discharge are set based on initial experiments [21, 22], which show that the device operates properly within this range. Finally, the charge current density is set higher than the discharge current density as suggested in [23], to make up for any lost capacity in the nickel electrode during discharge.

The electrolyte used in this study was a one molar (1 M) KOH solution. This concentration is notably lower compared to the values suggested in the open literature [2, 7, 23]. It was observed that the zinc plate corrodes rapidly at higher concentrations, severely limiting testing capabilities. The selected concentration has lower ionic conductivity resulting in higher internal resistance and lower capacity. However, it allows device testing and comparison between the different configurations for more extended periods of time.

## 5. Results and discussion

### 5.1. Charge–discharge response

The charge–discharge curve of a TMV microbattery with an active area of  $0.64 \text{ cm}^2$  and a cavity height of  $65 \mu\text{m}$  is shown in figure 8. The device is cycled according to the parameters shown in table 2 and its capacity is calculated within the

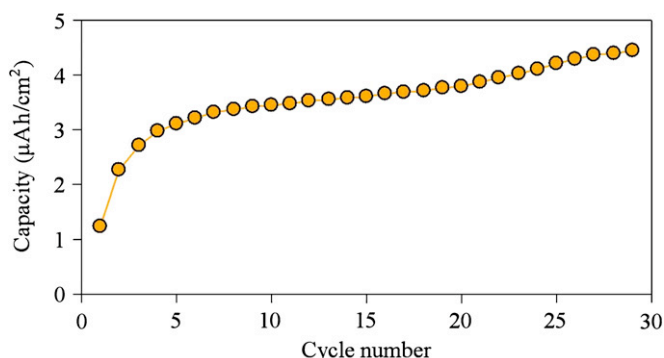


**Figure 9.** Capacity versus cycle number for a TMV modified device with a  $0.64 \text{ cm}^2$  active area and an electrode spacing of  $65 \mu\text{m}$ .

range of 2–1.3 V. The graph shows the first eight cycles of operation, where the capacity increases gradually from  $1.22 \mu\text{Ah cm}^{-2}$  to  $3.38 \mu\text{Ah cm}^{-2}$ . This particular device operated successfully for 30 cycles reaching a capacity of  $4.45 \mu\text{Ah cm}^{-2}$ , until testing was stopped manually. During repeated cycling, more nickel is converted to nickel oxide and nickel oxyhydroxide increasing the amount of the surface area that participates in the reaction. This results in an increase in the time of discharge and consequently in microbattery capacity. The capacity versus cycle number for this device is plotted in figure 9.

### 5.2. Effect of TMV coating

Devices with and without viral nanostructures were compared to investigate the effect of the increased surface area. Figure 10 shows the first discharge for three TMV modified and three unmodified devices (active area of  $0.64 \text{ cm}^2$ , electrode gap of  $65 \mu\text{m}$ ). The average discharge capacity for the nanostructured microbatteries is increased by a factor of 6 compared to the average capacity of those with planar nickel cathodes.

Testing of several identical nanostructured devices demonstrated that, while battery capacity is similar during the first cycle, discrepancies can be observed thereafter. In some of the devices tested the upper voltage limit of the potentiostat was reached, the cycling behavior became increasingly erratic and the capacity degraded abruptly. This behavior is primarily

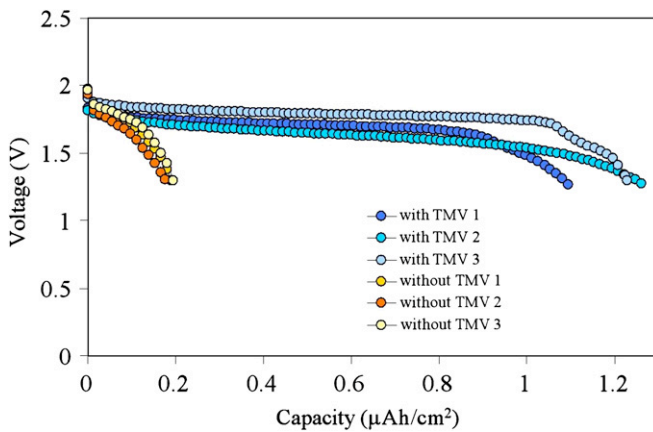


**Figure 10.** Initial discharges of cells with and without TMV coatings.

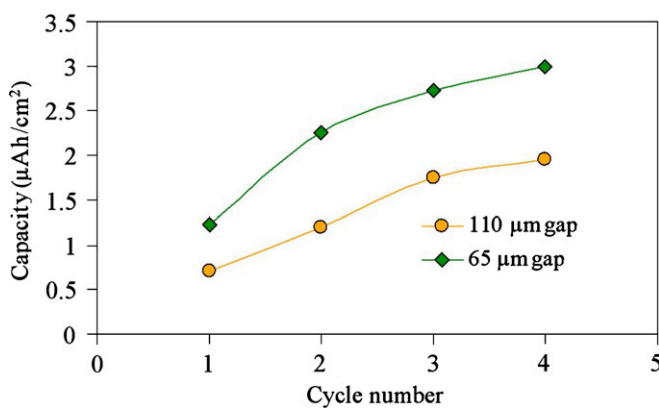


**Figure 11.** Capacity versus cycle number for devices with different electrode spacings.

attributed to variability in the as-fabricated devices, such as the surface quality of the zinc plate, the thickness of the nickel coating and improper sealing introduced during bonding. In figure 10, it is observed that the operating voltage of the microbatteries remains mostly in the range of 1.7 V. According to the discussion in section 2.2, this implies that more of the nickel hydroxide is present on the surface of the cathode, which is caused by temperature-induced effects during baking of the assembled devices.

### 5.3. Effect of the electrode gap

Devices with different cavity heights were tested to investigate the effect of electrode spacing. Figure 11 shows the capacity versus cycle number for electrode spacings of 65  $\mu\text{m}$  and 110  $\mu\text{m}$ . It is observed that a decrease in electrode spacing by roughly a factor of 2 results in an approximately equivalent increase in capacity in the working range of 2–1.3 V. The decreased gap between the anode and cathode causes a drop in the internal resistance within the electrolyte and increases the operating voltage of the cell, thus increasing its capacity in the range of interest.

### 5.4. Limitations and continued work

Common problems encountered in nickel–zinc batteries involve zinc corrosion in the alkaline electrolyte and uneven redistribution of chemical byproducts on the anode, leading to dendrite formation [23, 24]. Rapid zinc degradation was observed in many of the devices tested for this work, preventing cells from reaching the maximum capacity. Examination of the electrode surfaces after testing showed the formation of a substantial passivation layer on the zinc anode, which causes an increase in cell resistance during charge. In these cases, the upper voltage limit of the potentiostat was reached before the devices were fully charged and the capacity of the battery dropped rapidly. This is attributed to the lower available surface area of the zinc electrode, as compared to the nanostructured nickel cathode. Additionally, variability in the fabrication process is believed to be a significant factor contributing to inconsistencies in device operation.

To address these limitations, future work will focus on improving the anode and the fabrication process. The benefit of the TMV coatings can be fully realized by incorporating high aspect ratio nanostructures on the zinc electrode as well. The development of such a high surface area and high conductivity anode will result in increased capacity while reducing the effects of passivation. Moreover, TMV processing at the wafer level and alternative packaging methods are expected to increase the yield of the devices.

## 6. Conclusion

The first successful demonstration of a MEMS battery utilizing viral nanostructures was presented in this paper. Self-assembly and nickel coating of the *Tobacco mosaic virus* have been integrated into traditional MEMS fabrication processes, and nickel–zinc microbatteries with nanostructured cathodes have been developed and characterized. The TMV modified devices exhibit appropriate charge–discharge behavior for several cycles of operation, which vary from device to device. Corrosion of the zinc electrode and short-circuiting due to fabrication imperfections were observed to affect the operation of the microbatteries, which were tested until their lifetime was exhausted. The initial capacity of the nanostructured batteries was improved by a factor of 6 compared to cells without viral nanostructures. TMV microbatteries with smaller electrode spacings show an increase in capacity, which demonstrates the importance of the electrode gap as a design parameter. These results, combined with the simplicity of the viral self-assembly and metallization process, show the feasibility of developing more compact high-performance energy storage devices using this technology.

## Acknowledgments

This work is supported in part by the Laboratory for Physical Sciences (LPS) at the University of Maryland and DOE FG0202ER45975. The authors would like to thank Professor Peter Kofinas and Mr Ayan Ghosh from the Fischell Department of Bioengineering for assisting with

data acquisition and the staff at LPS and the Maryland Nanocenter for providing access to their clean-room facilities and metrology tools.

## References

- [1] Lee K B and Lin L 2003 Electrolyte-based on demand and disposable microbattery *J. Microelectromech. Syst.* **12** 840–7
- [2] Humble P H, Harb J N and LaFollete R 2001 Microscopic nickel-zinc batteries for use in autonomous microsystems *J. Electrochem. Soc.* **148** A1357–61
- [3] Bates J B, Dudney N J, Neudecker B, Ueda A and Evans A D 2000 Thin-film lithium and lithium-ion batteries *Solid State Ion.* **135** 33–45
- [4] West W C, Whitacre J F, White V and Rantakumar B V 2002 Fabrication and testing of all solid-state microscale lithium batteries for microspacecraft applications *J. Micromech. Microeng.* **12** 58–62
- [5] Long J W, Dunn B, Rolison D R and White H S 2004 Three dimensional battery architectures *Chem. Rev.* **104** 4463–92
- [6] Wang C, Taherabadi L, Jia G, Madou M, Yeh Y and Dunn B 2004 C-MEMS for the manufacture of 3D microbatteries *Electrochem. Solid-State Lett.* **7** A435–8
- [7] Chamran F, Yeh Y, Min H S, Dunn B and Kim C J 2007 Fabrication of high-aspect-ratio electrode arrays for three dimensional microbatteries *J. Microelectromech. Syst.* **16** 844–52
- [8] Zhang Z, Dewan C, Kothari S, Mitra S and Teeters D 2005 Carbon nanotubes synthesis, characteristics, and microbattery applications *Mater. Sci. Eng. B* **116** 363–8
- [9] Pushparaj V L *et al* 2007 Flexible energy storage devices based on nanocomposite paper *Proc. Natl Acad. Sci.* **104** 13574–7
- [10] Yuah Y F, Tu J P, Wu H M, Li Y and Shi D Q 2005 Size and morphology effects of ZnO anode nanomaterials for Zn/Ni secondary batteries *Nanotechnology* **16** 803–8
- [11] Nam K T, Kim D W, Yoo P J, Chiang C Y, Meethong N, Hammond P T, Chiang Y M and Belcher A M 2006 Virus-enabled synthesis and assembly of nanowires for lithium ion battery electrodes *Science* **312** 885–8
- [12] Royston E, Ghosh A, Kofinas P, Harris M T and Culver J N 2008 Self-assembly of virus-structured nanomaterials and their application as battery electrodes *Langmuir* **24** 906–12
- [13] Dujardin E, Peet C, Stubbs G, Culver J N and Mann S 2003 Organization of metallic nanoparticles using tobacco mosaic virus templates *Nano Lett.* **3** 413–7
- [14] Lee S Y, Royston E, Culver J N and Harris M T 2005 Improved metal cluster deposition on a genetically engineered *Tobacco Mosaic Virus* template *Nanotechnology* **16** S435–41
- [15] Yi H *et al* 2005 Patterned assembly of genetically modified viral nanotemplates via nucleic acid hybridization *Nano Lett.* **5** 1931–6
- [16] Dawson W O, Beck D L, Knorr D A and Grantham G L 1986 cDNA cloning of the complete genome of tobacco mosaic virus and production of infectious transcripts *Proc. Natl Acad. Sci.* **83** 1832–6
- [17] Gooding G V and Hebert T T 1967 A simple technique for purification of tobacco mosaic virus in large quantities *Phytopathology* **57** 1285
- [18] Knez M, Bittner A M, Boes F, Wege C, Jeske H, Maiß E and Kern K 2003 Bio-template synthesis of 3-nm nickel and cobalt nanowires *Nano Lett.* **3** 1079–82
- [19] Knez M, Sumser M, Bittner A M, Wege C, Jeske H, Kooi S, Burghard M and Kern K 2002 Electrochemical modification of individual nano-objects *J. Electroanal. Chem.* **522** 70–4
- [20] Anhoj T A, Jorgensen A M, Zauner D A and Hubner J 2006 The effect of soft bake temperature on the polymerization of SU-8 photoresist *J. Micromech. Microeng.* **16** 1819–24
- [21] Gerasopoulos K, McCarthy M, Royston E, Culver J N and Ghodssi R 2007 Nanostructured nickel zinc microbatteries using the *tobacco mosaic virus* *Proc. 7th Int. Workshop on Micro and Nano Technology for Power Generation and Energy Conversion Applications (PowerMEMS 2007) (Freiburg, Germany)* pp 347–50
- [22] Gerasopoulos K, McCarthy M, Royston E, Culver J N and Ghodssi R 2008 Microbatteries with tobacco mosaic virus templated electrodes *21st IEE Int. Conf. Micro Electro Mechanical Systems (MEMS 2008) (Tucson, az) 2008* 960–3
- [23] Linden D 1984 *Handbook of Batteries and Fuel Cells* (New York: McGraw-Hill)
- [24] McLarnon F R and Cairns E J 1991 The secondary alkaline zinc electrode *J. Electrochem. Soc.* **138** 645–64